Scientific Research

Threshold Characteristics Enhancement of a Single Mode 1.55 μm InGaAsP Photonic Crystal VCSEL for Optical Communication Systems

Abbas Majdabadi[1], Saeid Marjani[2*], Masoud Sabaghi[1]

[1]Laser and Optics Research School, Nuclear Science and Technology Research Institute (NSTRL), Tehran, Iran
[2]Department of Electrical Engineering, Ferdowsi University of Mashhad, Mashhad, Iran
Email: *saeid.marjani@stu.um.ac.ir, *saeid.marjani.2015@ieee.org

Abstract

In the present work, we investigate threshold characteristics of a single mode 1.55 μm InGaAsP vertical cavity surface emitting laser (VCSEL) with two different optical confinement structures. The device employs InGaAsP active region, which is sandwiched between GaAs/AlGaAs and GaAs/AlAs distributed Bragg reflectors (DBRs). The optical confinement introduced by the oxide aperture or a single defect photonic crystal design with holes etched throughout the whole structure, is compared with previous work. Photonic crystal VCSEL shows 30.86% and 57.02% lower threshold current than that of the similar oxide confined VCSEL and previous results, respectively. This paper provides key results of the threshold characteristics, including the threshold current and the threshold power. Results suggest that, the 1.55 μm InGaAsP photonic crystal VCSEL seems to be the most optimal one for light sources in high performance optical communication systems.

Keywords

Threshold Characteristics, Single Mode, VCSEL, Optical Communication Systems

1. Introduction

In recent years, the vertical cavity surface emitting lasers (VCSELs) have attracted extremely [1]. VCSEL is one of the key light source used in high performance optical communication systems where single mode operation,

---

*Corresponding author.

high output power, high speed modulation and low manufacture cost are necessary [2]. High optical gain in the active area, high temperature, low threshold current and high thermal conductivity in the reflecting mirrors are the main difficulties in developing VCSELs which are used in the field of optical spectroscopy [3]. When all lateral modes except one are suppressed, a fully single mode, VCSEL operation is achieved. Mainly, a single lobe distribution in a desirable lateral direction defined lasing of the fundamental mode. If carriers are confined to the central part of the device, this modal distribution has best overlaps with the gain radial distribution. In real device, the injected current is far from the central part of the device where the fundamental mode has appreciable amplitude. Consequently, it is necessary to funnel the current into the center of the active region. There have been several approaches to address this issue: selective oxidation [4], proton implantation [5] or structured tunnel junction [6]. On one hand, narrowing the current aperture causes the reduction of the emitted power and on the other hand, broadening of the current aperture favors multimode operation. Hence, it is necessary to additional structuring of VCSELs for their single mode operation with broader current apertures. It can be assured by anti-resonant profile of the refractive index in the distributed Bragg reflectors (DBRs) [7], surface etching [8], surface grating [9] and photonic crystals (PhC) [10]. Since PhC has already verified its ability to select very narrow spectrum of allowed frequencies and discriminate all higher modes [11], it is extremely attractive.

From one side, the PhC improves the wave guiding, which leads to better mode confinement and hence, to higher efficiency of the stimulated recombination. From another side, it destroys the reflectivity of the DBR. The accurate design can balance between these two effects and improve the device efficiency in terms of reduction of the threshold current and increase of lateral mode discrimination.

Recently, we proposed a structure for decreasing the threshold current of VCSELs [12] and showed that proposed structure decreased the threshold current about 76.52% from 2.3 mA to 0.6 mA. There have been a number of reports on the effect of the photonic crystal confined (PhC) on the modal characteristics by Czyszanowski's group [13]-[15]. However, the structures presented are different laser wavelength (1.3 μm), the etching depth and simulation method (the plane-wave admittance method).

In this paper, the impact of the photonic crystal confined and oxide confined (OC) optical confinement schemes on the threshold characteristics of single mode 1.55 μm InGaAsP VCSEL design similar to that reported in [4] is investigated and compared with previous results [12] [14] [15]. The paper is organized as follows: Section 2 briefly describes the theoretical model; Section 3 provides the details of the VCSEL structures; and Section 4 presents the obtained numerical results. Finally, in Section 5, we conclude.

2. Theory

In modeling VCSEL, we must the electrical, optical and thermal interaction during VCSEL performance [16]. Thus base of simulation is to solve Poisson and continuity equations for electrons and holes. Poisson's equation is defined by [17]:

$$\nabla \cdot (\varepsilon \nabla \Psi) = \rho \tag{1}$$

where ψ is electrostatic potential, ρ is local charge density and ε is local permittivity. The continuity equations of electron and hole are given by [17]:

$$\frac{\partial n}{\partial t} = G_n - R_n + \frac{1}{q} \nabla \cdot \overrightarrow{J_n}, \tag{2}$$

$$\frac{\partial p}{\partial t} = G_p - R_p + \frac{1}{q} \nabla \cdot \overrightarrow{J_p}. \tag{3}$$

where n and p are the electron and hole concentration, J_n and J_p are the electron and hole current densities, G_n and G_p are the generation rates for electrons and holes, R_n and R_p are the recombination rates and q is the magnitude of electron charge.

The fundamental semiconductor Equations (1)-(3) are solved self-consistently together with Helmholtz and the photon rate equations. The applied technique for solution of Helmholtz equation is based on effective frequency method [18] which shows accuracy for great portion of preliminary problems. Two-dimensional Helmholtz equation is solved to determine the transverse optical field profile and it is given by [17]:

$$\nabla^2 E(r,z,\varphi) + \frac{\omega_0}{c^2} \varepsilon(r,z,\varphi,\omega) E(r,z,\varphi) = 0 \tag{4}$$

where ω is the frequency, $\varepsilon(r,z,\varphi,\omega)$ is the complex dielectric permittivity, $E(r,z,\varphi)$ is the optical electric field and c is the speed of light in vacuum.

The light power equation relates electrical and optical models. The photon rate equation is given by [17]:

$$\frac{\mathrm{d}S_m}{\mathrm{d}t} = \left(\frac{c}{N_{\text{eff}}} G_m - \frac{1}{\tau_{\text{phm}}} - \frac{cL}{N_{\text{eff}}} \right) S_m + R_{\text{spm}} \tag{5}$$

where S_m is the photon number, G_m is the modal gain, R_{spm} is the modal spontaneous emission rate, L represents the losses in the laser, N_{eff} is the group effective refractive index, τ_{phm} is the modal photon lifetime and c is the speed of light in vacuum. The m refers to the modal number.

The heat flow equation has the form [17]:

$$C \frac{\partial T_L}{\partial t} = \nabla(\kappa \nabla T_L) + H \tag{6}$$

where C is the heat capacitance per unit volume, κ is the thermal conductivity, H is the generation, T_L is the local lattice temperature and H is the heat generation term.

The heat generation equation has the form [17]:

$$H = \left[\frac{\overrightarrow{|J_n|^2}}{q\mu_n n} + \frac{\overrightarrow{|J_p|^2}}{q\mu_p p} \right] + q(R-G)\left[\phi_p - \phi_n + T_L(P_p - P_n) \right] - T_L\left(\overrightarrow{J_n}\nabla P_n + \overrightarrow{J_p}\nabla P_p \right) \tag{7}$$

where: $\left[\dfrac{\overrightarrow{|J_n|^2}}{q\mu_n n} + \dfrac{\overrightarrow{|J_p|^2}}{q\mu_p p} \right]$ is the Joule heating term; $q(R-G)\left[\phi_p - \phi_n + T_L(P_p - P_n) \right] - T_L\left(\overrightarrow{J_n}\nabla P_n + \overrightarrow{J_p}\nabla P_p \right)$ is

the recombination and generation heating and cooling term; and the Peltier and Thomson effects.

In addition, all important, usually non-linear, interactions between the optical, electrical, thermal and recombination phenomena are also taken into account with the aid of the self-consistent iteration algorithm, including: gain-induced wave-guiding, thermal focusing, self-focusing, temperature dependence of optical gain and absorption coefficients and the energy gaps and electrical conductivities and thermal conductivities, carrier-concentration dependence of electrical conductivities and optical gain and absorption coefficients and the energy gaps and wavelength dependences of optical gain and absorption coefficients. Consequently, several factors are effective in determining the profiles of all model parameters within the whole VCSEL volume, including: different chemical compositions of the VCSEL layers, the distributions of the temperature, the current density, the carrier concentration and the mode radiation intensity.

Heat loss from the modeled VCSEL device was specified using thermal contacts at the top electrode, bottom electrode and the device sidewall. The thermal contacts define thermal conductivities to simulate heat loss from radiation via exposed surfaces or conduction through the semiconducting material to a heatsink.

Equation (1)-(7) provide an approach that can account for the mutual dependence of electrical, thermal, optical and elements of heat sources. In this paper, we employ numerical-based simulation software to assist in the device design and simulation [17].

3. VCSEL Structure

The analyzed structure is similar to the one recently reported in [12] has been chosen as a model structure for the analysis of the 1.55 µm InGaAsP VCSEL. The active region consists of six quantum wells where the well is 5.5 nm $In_{0.76}Ga_{0.24}As_{0.82}P_{0.18}$ and the barrier is 8 nm $In_{0.48}Ga_{0.52}As_{0.82}P_{0.18}$. In both sides of this active region, there is InP and on top of it, GaAs. The top mirror is 30 layers of $GaAs/Al_{0.33}Ga_{0.67}As$ with index of refraction 3.38 and 3.05 respectively, and the bottom mirror has 28 layers of GaAs/AlAs with index of refraction 3.38 and 2.89 respectively. Layer thickness, doping, majority carrier mobility, refractive index, temperature coefficient of *n*, absorption coefficient, and thermal conductivity of layers are listed in **Table 1**. In the OC VCSEL, the incorporation of a high aluminum content layer ($Al_{0.98}Ga_{0.02}As$) in two DBR periods above the active region allows for selective oxidation [11]. **Figure 1(a)** shows the PhC VCSEL structure, which is similar to the above VCSEL [12] but made additionally with a single defect PhC etched throughout the whole structure. The optical confinement

x

Table 1. Parameters of the structure (l: layer thickness; N_{dop}: doping; μ: majority carrier mobility; n: refractive index; dn/dT: temperature coefficient of n; α: absorption coefficient; and κ: thermal conductivity).

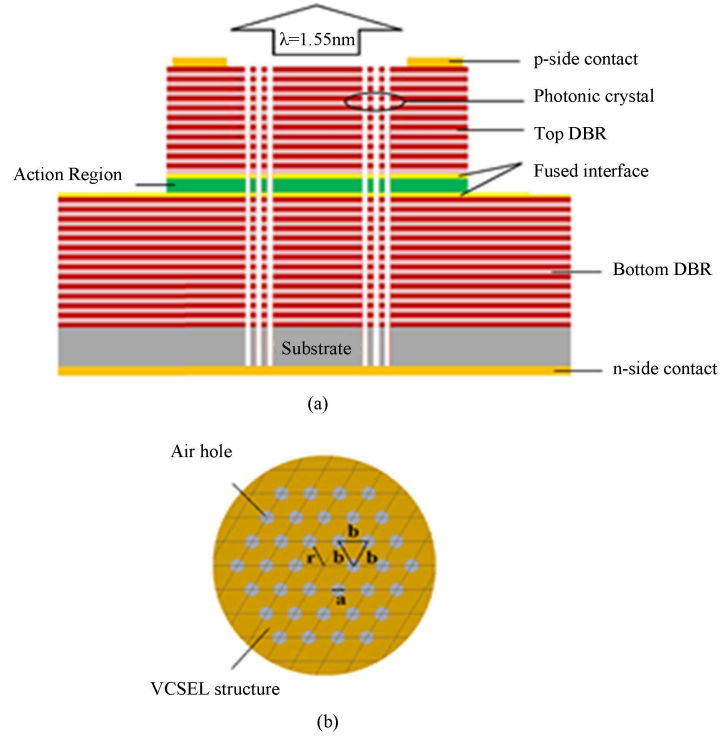| Parameter unit	l (µm)	N_{dop} (1/cm^3)	μ (cm^2/V·s)	n	dn/dT (10^{-4}/K)	α (1/cm)	κ (W/cm·K)
Au/Ti (contact)	0.200	-	-	0.83	-	684,000	0.67
p-GaAs	0.020	2×10^{19}	-	3.38	3	500	0.44
p-GaAs	0.182	4×10^{17}	-	3.38	3	25	0.22
p-Al$_{0.67}$Ga$_{0.33}$As (DBR)	0.127	4×10^{17}	-	3.05	2	25	0.22
p-GaAs (DBR)	0.115	4×10^{17}	-	3.38	3	25	0.44
p-GaAs (spacer)	0.020	4×10^{17}	-	3.38	3	25	0.44
p-GaAs (spacer)	0.010	4×10^{19}	-	3.38	3	1000	0.44
p-InP (spacer)	0.178	1×10^{18}	30	3.17	2	24	0.68
p-Inp (spacer)	0.100	1×10^{16}	150	3.17	2	0.24	0.68
In$_{0.76}$Ga$_{0.24}$As$_{0.82}$P$_{0.18}$ (QW)	0.0055	-	100	3.6	2	54	0.043
In$_{0.48}$Ga$_{0.52}$As$_{0.82}$P$_{0.18}$ (barrier)	0.008	-	100	3.4	2	54	0.043
n-InP (spacer)	0.258	5×10^{18}	4600	3.15	2	8	0.68
n-GaAs (spacer)	0.050	1×10^{18}	-	3.38	3	6	0.44
n-GaAs (DBR)	0.115	1×10^{18}	-	3.38	3	6	0.22
n-AlAs (DBR)	0.134	1×10^{18}	-	2.89	1	3	0.22
n-GaAs (substrate)	450	5×10^{18}	-	3.38	3	5.8	0.44

Figure 1. (a) Schematic structure of the VCSEL device and (b) top view of the triangular-lattice air holes pattern.

is achieved by means of seven air holes where the center is missed off to make the defect region, as shown in **Figure 1(b)**. The crucial PhC parameters are connected by the air hole diameter (a), the pitch (b) and the optical aperture diameter (r), are defined in **Figure 1(b)**. The transverse index guiding around the single defect region

can be controlled by the air hole diameter the pitch ratio (a/b). We fixed the optical aperture diameter at 2 μm and a/b ratio is varied from 0 to 0.95 for the study.

4. Results

The present work allows for determination of the optimum VCSEL structure that is found by a minimization of the threshold power and current. **Figure 2** presents a comparison of the optical intensity distributions at the lasing threshold of OC and PhC VCSELs with different a/b values that emphasize the overlap of the holes by the modes for the cutoff condition. Fundamentally, the increase of a/b ratio and the optical aperture diameter leads to an increase of the optical confinement factor within the active region and the optical intensity distributions changes significantly. The case of a/b = 0.3 shows a star-like shape of the PhC mode that the field permeates the absorptive surrounding regions. However, at higher values of a/b ratios the mode distributions remain almost unchanged.

A comparison of the threshold characteristics of OC, PhC VCSELs and previous work [12] [14] [15] as a function of the a/b ratio is presented in **Figures 3-5**. As can be seen from **Figure 3**, the logarithmically scaled threshold power of PhC VCSELs decrease gradually with the increase in the a/b ratio. This initial decrement (from a/b = 0 to a/b = 0.9) should be mainly due to improving the optical confinement by the photonic crystal. For a/b = 0.9 the threshold power reaches a minimum value of 0.5719e−5 W and then rapidly increases for a/b = 0.95, which should be mainly due to blocking of most of the current flow by the holes. The minimal threshold power is lowered by 48.82% from 1.1176e−5 W to 0.5719e−5 W than that of the OC VCSEL, since, the electrical resistance of the etched PhC regions is increased.

Figure 4 shows a monotonic decrease in the logarithmically scaled threshold current of PhC VCSELs with the increase in the a/b ratio. This is caused by more effective optical confinement and stronger limitation of the current flow to the active region. As shown in **Figure 4**, photonic crystal VCSEL shows 30.86% and 57.02% lower threshold current than that of the similar oxide confined VCSEL and previous results [19], respectively. Threshold current for two PhC VCSEL structures [14] [15] determined by $r = 4$ μm, a/b = 0.5 and $r = 8$ μm, a/b = 0.5 are 4.9 mA and 7.11 mA, respectively, which are very close to previous values of 4.89 mA and 7.12 mA, respectively [15]. We fixed the depth of the PhC holes at 7 μm for two PhC VCSEL structures.
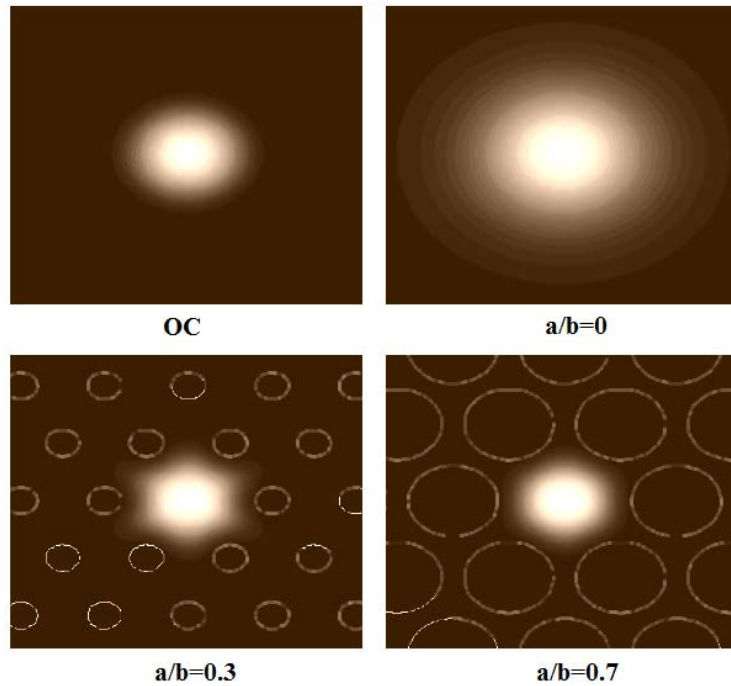

Figure 2. The optical intensity distributions at the lasing threshold of the fundamental mode within the active region in the case of the OC VCSEL and the PhC VCSEL for four different a/b ratios.
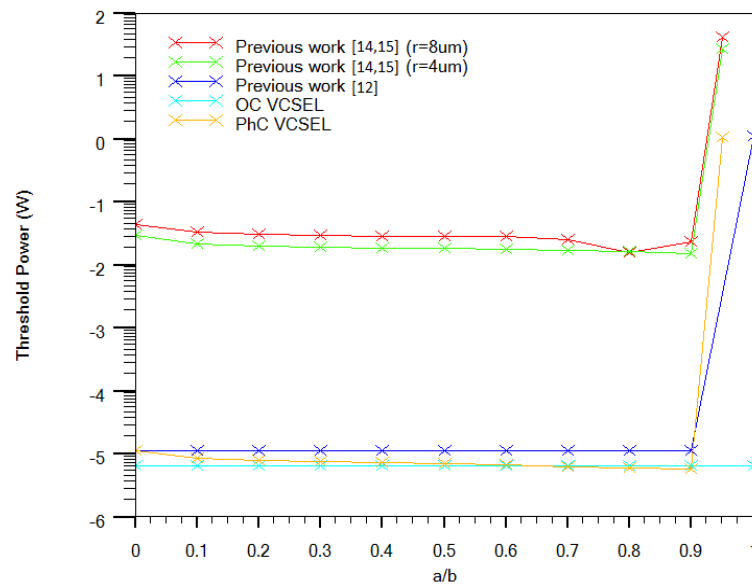
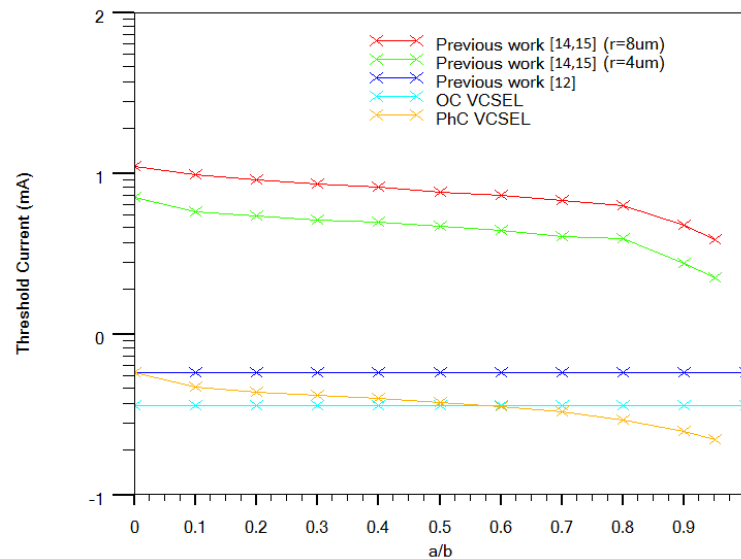**Figure 3.** Threshold power of OC, PhC VCSELs and previous work [12] [14] [15] as a function of the a/b ratio.

Figure 4. Threshold current of OC, PhC VCSELs and previous work [12] [14] [15] as a function of the a/b ratio.

Figure 5 shows a threshold temperature increase for a/b = 0 than that of the OC VCSEL, since, the thermal focusing is the unique wave guiding mechanism induced by the PhC structure. As can be seen from **Figure 5**, threshold temperature of the OC VCSEL is always smaller than that of the PhC VCSEL. This is caused by the more efficient heat sinking process in the OC VCSEL. For a/b = 0.7 the threshold temperature reaches a minimum value of 300.147 K that is the optimum configuration for over threshold operation.

5. Conclusion

Threshold characteristics of a single mode 1.55 µm InGaAsP vertical cavity surface emitting laser with two different optical confinement structures were analyzed and compared with previous work. In summary, the results indicate that lowest threshold current and threshold power is for a/b = 0.9 that shows 30.86% and 57.02%
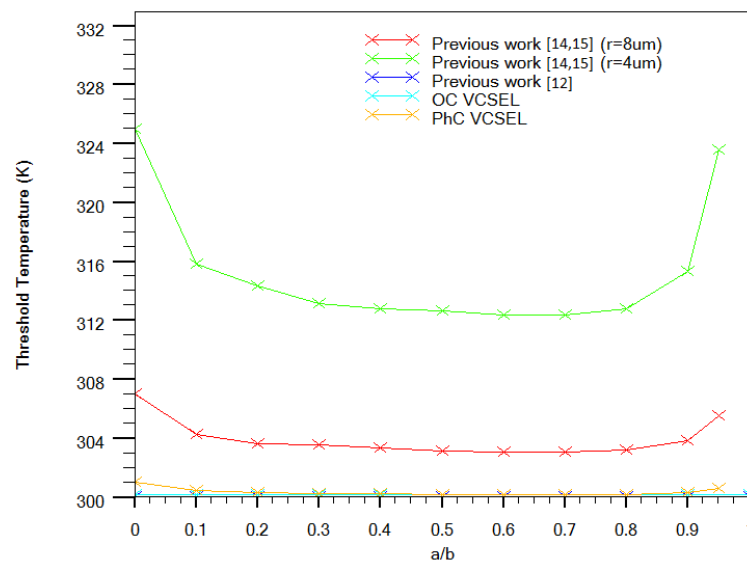
Figure 5. Threshold temperature of OC, PhC VCSELs and previous work [12] [14] [15] as a function of the a/b ratio.

lower threshold current than that of the similar oxide confined VCSEL and previous results, respectively. Our studies reveal that high-precision PhC etching is necessary in PhC VCSELs in order to optimize their threshold characteristics for light sources in high performance optical communication systems.

References

[1]   Iga, M.K. (2000) Surface-Emitting Laser—Its Birth and Generation of New Optoelectronic Field. *IEEE Journal of Selected Topics in Quantum Electronics*, **6**, 1201-1215. http://dx.doi.org/10.1109/2944.902168

[2]   Dems, M., Kotynski, R. and Panajotov, K. (2005) Plane Wave Admittance Method—A Novel Approach for Determining the Electromagnetic Modes in Photonic Structures. *Optics Express*, **13**, 3196-3207. http://dx.doi.org/10.1364/OPEX.13.003196

[3]   Kapon, E. and Sirbu, A. (2009) Long-Wavelength VCSELS Power-Efficient Answer. *Nature Photonics*, **3**, 27-29. http://dx.doi.org/10.1038/nphoton.2008.266

[4]   Jung, C., Jager, R., Grabherr, M., Schnitzer, P., Michalzik, R., Weigl, B., Muller, S. and Ebeling, K.J. (1997) 4.8 mW Single-Mode Oxide Confined Topsurface Emitting Vertical-Cavity Laser Diodes. *Electronics Letters*, **33**, 1790-1791. http://dx.doi.org/10.1049/el:19971207

[5]   Morgan, R.A., Guth, G.D., Focht, M.W., Asom, M.T., Kojima, K., Rogers, L.E. and Callis, S.E. (1993) Transverse Mode Control of Vertical-Cavity Top-Surface-Emitting Lasers. *IEEE Photonics Technology Letters*, **4**, 374-377. http://dx.doi.org/10.1109/68.212669

[6]   Long, C.M., Mutter, L., Dwir, B., Mereuta, A., Caliman, A., Sirbu, A., Iakovlev, V. and Kapon, E. (2014) Optical Injection Locking of Transverse Modes in 1.3-µm Wavelength Coupled-VCSEL Arrays. *Optics Express*, **22**, 21137-21144. http://dx.doi.org/10.1364/OE.22.021137

[7]   Zhou, D. and Mawst, L.J. (2002) High-Power Single-Mode Antiresonant Reflecting Optical Waveguide-Type Vertical-Cavity Surface-Emitting Lasers. *IEEE Journal of Quantum Electronics*, **38**, 1599-1606. http://dx.doi.org/10.1109/JQE.2002.805107

[8]   Debernardi, P., Unold, H.J., Maehnss, J., Michalzik, R., Bava, G.P. and Ebeling, K.J. (2003) Single-Mode, Single-Polarization VCSELs via Elliptical Surface Etching: Experiments and Theory. *IEEE Journal of Selected Topics in Quantum Electronics*, **9**, 1394-1404. http://dx.doi.org/10.1109/JSTQE.2003.819487

[9]   Haglund, A., Gustavsson, J.S., Bengtsson, J., Jedrasik, P. and Larsson, A. (2006) Design and Evaluation of Fundamental-Mode and Polarization-Stabilized VCSELs with a Subwavelength Surface Grating. *IEEE Journal of Quantum Electronics*, **42**, 231-240. http://dx.doi.org/10.1109/JQE.2005.863703

[10] Siriani, D.F., Tan, M.P., Kasten, A.M., Lehman Harren, A.C., Leisher, P.O., Sulkin, J.D., Raftery Jr., J.J., Danner, A.J., Giannopoulos, A.V. and Choquette, K.D. (2009) Mode Control in Photonic Crystal Vertical-Cavity Surface-Emitting Lasers and Coherent Arrays. *IEEE Journal of Selected Topics in Quantum Electronics*, **15**, 909-917.

http://dx.doi.org/10.1109/JSTQE.2008.2012121

[11] De La Rue, R. (2006) Photonic Crystal Components: Harnessing the Power of the Photon. *Optics and Photonics News*, **17**, 30-35. http://dx.doi.org/10.1364/OPN.17.7.000030

[12] Faez, R., Marjani, A. and Marjani, S. (2011) Design and Simulation of a High Power Single Mode 1550 nm InGaAsP VCSELs. *IEICE Electronics Express*, **8**, 1096-1101. http://dx.doi.org/10.1587/elex.8.1096

[13] Czyszanowski, T., Dems, M., Sarzala, R., Nakwaski, W. and Panajotov, K. (2011) Precise Lateral Mode Control in Photonic Crystal Vertical-Cavity Surface-Emitting Lasers. *IEEE Journal of Quantum Electronics*, **99**, 1291-1296. http://dx.doi.org/10.1109/JQE.2011.2159363

[14] Czyszanowski, T., Dems, M., Thienpont, H. and Panajotov, K. (2008) Modal Gain and Confinement Factors in Top- and Bottom-Emitting Photonic-Crystal VCSEL. *Journal of Physics D*: *Applied Physics*, **41**, Article ID: 085102. http://dx.doi.org/10.1088/0022-3727/41/8/085102

[15] Czyszanowski, T. (2009) Discrimination of Higher-Order Modes in Photonic-Crystal VCSEL. *Proceedings of the IEEE/LEOS Winter Topicals Meeting Series*, Innsbruck, 12-14 January 2009, 20-21.

[16] Menon, P.S., Kumarajah, K., Ismail, M., Majlis, B.Y.M. and Shaari, S. (2010) Long-Wavelength MQW Vertical-Cavity Surface Emitting Laser: Effects of Lattice Temperature. *Journal of Optical Communications*, **31**, 81-84. http://dx.doi.org/10.1515/JOC.2010.31.2.81

[17] SILVACO International Incorporated (2010) ATLAS User's Manual. Version 5.12.0.R., SILVACO, Inc., USA.

[18] Wenzel, H. and Wunsche, H.-J. (1997) The Effective Frequency Method in the Analysis of Vertical-Cavity Surface-Emitting Lasers. *IEEE Journal of Quantum Electronics*, **33**, 1156-1162. http://dx.doi.org/10.1109/3.594878

[19] Choquette, K.D., Geib, K.M., Ashby, C.I., Twesten, R.D., Blum, O., Hou, H.Q., Follstaedt, D.M., Hammons, B.E., Mathes, D. and Hull, R. (1997) Advances in Selective Wet Oxidation of AlGaAs Alloys. *IEEE Journal of Selected Topics in Quantum Electronics*, **3**, 916-926. http://dx.doi.org/10.1109/2944.640645

Scientific Research Publishing (SCIRP) is one of the largest Open Access journal publishers. It is currently publishing more than 200 open access, online, peer-reviewed journals covering a wide range of academic disciplines. SCIRP serves the worldwide academic communities and contributes to the progress and application of science with its publication.

Other selected journals from SCIRP are listed as below. Submit your manuscript to us via either submit@scirp.org or Online Submission Portal.